
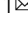


A quantum battery with quadratic driving

Charles Andrew Downing¹   & Muhammad Shoufie Ukhtary^{1,2}

Quantum batteries are energy storage devices built using quantum mechanical objects, which are developed with the aim of outperforming their classical counterparts. Proposing optimal designs of quantum batteries which are able to exploit quantum advantages requires balancing the competing demands for fast charging, durable storage and effective work extraction. Here we study theoretically a bipartite quantum battery model, composed of a driven charger connected to an energy holder, within two paradigmatic cases of a driven-dissipative open quantum system: linear driving and quadratic driving. The linear battery is governed by a single exceptional point which splits the response of the battery into two regimes, one of which induces a good amount of useful work. Quadratic driving leads to a squeezed quantum battery, which generates plentiful useful work near to critical points associated with dissipative phase transitions. Our theoretical results may be realized with parametric cavities or nonlinear circuits, potentially leading to the manifestation of a quantum battery exhibiting squeezing.

¹Department of Physics and Astronomy, University of Exeter, Exeter EX4 4QL, UK. ²Research Center for Quantum Physics, National Research and Innovation Agency (BRIN), South Tangerang 15314, Indonesia. ✉email: c.a.downing@exeter.ac.uk

The Laws of Thermodynamics allow for a complete description of classical thermal machines, from classical heat engines to refrigerators. However, the ongoing trend for device miniaturisation inevitably led to quantum effects becoming important. This realisation required the development of theories of thermal energy conversion in the quantum regime^{1,2}. Shortly afterwards, an influential study of energy storage and transduction at the nanoscale pioneered the concept of a quantum system storing and releasing energy on demand: a quantum battery^{3,4}.

An archetypal quantum battery model consists of two parts, the battery holder and the battery charger. The holder is essentially isolated from the external environment in order to prevent energy loss, and hence it is modelled as a dissipationless subsystem. In order to receive energy, the battery holder then needs to be coupled to the battery charger. The charger subsystem is supposed to feel the environment—allowing it to be driven—but this comes at the cost of the charger suffering from dissipation. After charging for some finite period of time, the battery holder is disconnected from the battery charger so that energy storage, and eventually energy extraction on demand, may occur⁵. This fundamental bipartite quantum battery model, along with its charging, storage and discharging performances, has been considered theoretically in various guises over the last few years of intensive quantum battery research^{6–23}.

Experimentally, superabsorption in a Dicke-style quantum battery has already been reported²⁴, as has a detailed investigation of collective charging in a variety of spin-based systems²⁵. The realisation of a quantum battery based upon a superconducting qutrit, including a characterisation of its charging and self-discharging processes, has also been achieved in some recent and rather ingenious experiments²⁶. Meanwhile, the first steps in gauging the performance of quantum emitters and light fields for the purpose of energy transfer have been performed empirically²⁷. Complementary studies of the energetics of various quantum objects, including qubits^{28,29} and nuclear spins³⁰, demonstrate the promise of this nascent quantum technological field.

In what follows, we consider theoretically the celebrated bipartite quantum battery model, where the battery charger and battery holder are modelled as two coupled quantum harmonic oscillators, in two different circumstances. Firstly, we revisit the linear (one-photon) driving setup as discussed by Farina and co-workers⁵. This study lays the theoretical framework for the Gaussian quantum batteries considered and acts as a comparator for the second case of interest: a quadratic (two-photon) driving arrangement^{31–35}. The latter case of parametric driving significantly alters the underlying physics of the quantum battery

due to the inducement of spectral collapse, quantum squeezing, dynamic instabilities and dissipative phase transitions. Most importantly, we reveal that the quadratic quantum battery allows for abundant useful energy to be stored in it when the driving amplitude is near certain critical values.

Results

Bipartite quantum battery model. The total Hamiltonian operator \hat{H} of the composite quantum battery system can be decomposed into four parts,

$$\hat{H} = \hat{H}_c + \hat{H}_h + \hat{H}_{c-h} + \hat{H}_d, \tag{1}$$

which accounts for the battery charger energy, the battery holder energy, the charger-holder coupling and the coherent driving of the charger, respectively. Taking $\hbar = 1$ throughout, these Hamiltonian contributions are—each in turn—defined by

$$\hat{H}_c = \omega_b c^\dagger c, \tag{2}$$

$$\hat{H}_h = \omega_b h^\dagger h, \tag{3}$$

$$\hat{H}_{c-h} = g (c^\dagger h + h^\dagger c), \tag{4}$$

$$\hat{H}_d = \Omega e^{i\theta} e^{-i\omega_d t} c^\dagger + \text{h.c.} . \tag{5}$$

The energy level spacings of the harmonic oscillators modelling the battery charger and the battery holder are equal at ω_b , the coupling strength between them is g , and the laser driving the charger has an amplitude $\Omega \geq 0$, phase θ and frequency ω_d . Excitations in the battery charger are created and destroyed by the operators c^\dagger and c , respectively, while the ladder operators h^\dagger and h track the transitions up and down the energy ladder of the battery holder. Both flavours of the operator are subject to bosonic commutation relations, $[c, c^\dagger] = 1$ and $[h, h^\dagger] = 1$. Notably, the counter-rotating terms $\propto ch$ and $\propto c^\dagger h^\dagger$ not appearing in the coupling Hamiltonian of Eq. (4) have been dropped since they are small for typical couplings g satisfying $g \ll \omega_b$. Therefore, we do not enter the so-called ultrastrong coupling regime, as commonly defined without reference to losses^{36–39} (see also Supplementary Notes 2 and 3, where we find that this rotating-wave approximation is a good one for any coupling g satisfying $g \lesssim \omega_b/1000$). A graphical representation of this bipartite battery arrangement, as captured mathematically by Eq. (1), is sketched in Fig. 1a. This cartoon includes the three key parameters of the model: the driving amplitude Ω , the charger-holder coupling g , and the loss rate of the charger γ .

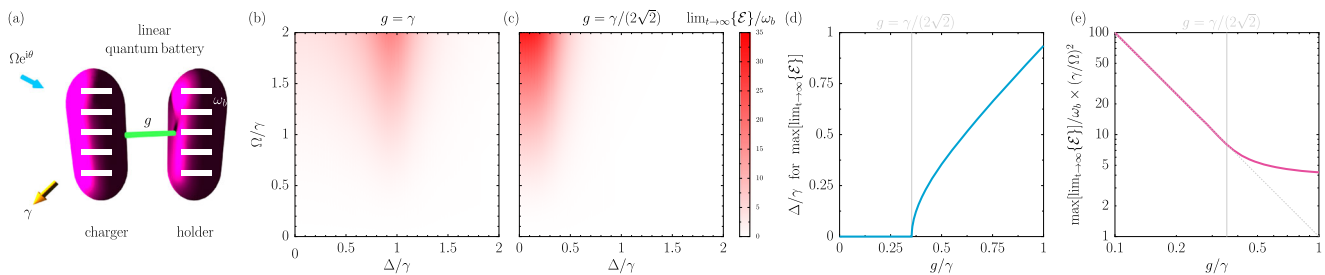


Fig. 1 The linear quantum battery and its steady state. Panel **a**: a sketch of the bipartite quantum battery (both parts are modelled as quantum harmonic oscillators, with the level spacing ω_b), composed of a battery charger coupled to a battery holder with the coupling strength g (green bar). The charger is driven coherently (cyan arrow) with an amplitude Ω , phase θ and frequency ω_d , while it suffers a loss (yellow arrow) at the decay rate γ . Panel **b**: the ergotropy \mathcal{E} in the steady state (in units of ω_b) as a function of Ω and Δ (both in units of γ) from Eq. (16). Here the coupling $g = \gamma$. Panel **c**: as for panel **b**, but with $g = \gamma/(2\sqrt{2}) \simeq 0.35\gamma$. Panel **d**: the detuning Δ associated with the maximum of the steady state ergotropy \mathcal{E} , as a function of the coupling g [cf. Eq. (17)]. Panel **e**: a semi-logarithmic plot of the maximum of the steady state ergotropy \mathcal{E} , in units of ω_b and scaled by $(\gamma/\Omega)^2$, as a function of the coupling g [cf. Eq. (18)].

While the battery holder is approximated as a dissipationless subsystem, we consider the battery charger subsystem to suffer loss (as measured with the decay rate γ , where $\gamma \geq 0$). Within an open quantum systems approach^{40,41}, we employ the Gorini–Kossakowski–Sudarshan–Lindblad quantum master equation for the density matrix ρ , in the standard form $\partial_t \rho = i[\rho, \hat{H}] + (\gamma/2)\mathcal{L}_c[\rho]$. Here the Lindbladian superoperator $\mathcal{L}_c[\rho] = 2c\rho c^\dagger - c^\dagger c\rho - \rho c^\dagger c$ acts on ρ , while the unitary dynamics of the closed system are provided by the Hamiltonian operator \hat{H} of Eq. (1). In arriving at this master equation, we have employed the Born approximation (due to the assumption of weak interactions between the system and the environment), the Markov approximation (due to the supposition that the memory of the environment is much shorter than that of the system), and the secular approximation (due to certain transition frequencies leading to quickly-rotating terms which are neglectable)⁴⁰.

In order to judge the energetic performance of the quantum battery there are two crucial energies of interest, E_h and E_h^β , which are both associated with the battery holder⁵

$$E_h = \text{Tr}\{\hat{H}_h \rho_h\}, \tag{6}$$

$$E_h^\beta = \text{Tr}\{\hat{H}_h \rho_h^\beta\}, \tag{7}$$

here the reduced density matrix ρ_h of the battery holder subsystem h is defined by $\rho_h = \text{Tr}_c\{\rho\}$, where the partial trace over the battery charger subsystem c has been taken. The quantity E_h in Eq. (6) measures the mean energy stored in the battery holder due to the state ρ_h . However, not all of this energy E_h may be useful (for example, the system may be in thermal equilibrium). The state ρ_h^β appearing in Eq. (7) is the so-called passive state of the battery holder, which has the property that no work can be extracted from it cyclically under unitary evolution^{42–44}. The passive state ρ_h^β can be obtained by re-ordering the eigenvalues of the Hamiltonian and density matrix appropriately⁴⁵. The energies of Eq. (6) and Eq. (7) may then be simply combined into an influential measure—the so-called ergotropy \mathcal{E} —like so

$$\mathcal{E} = E_h - E_h^\beta, \tag{8}$$

which measures the upper bound of the useful energy stored within the battery holder⁴⁵. The ergotropy \mathcal{E} will be nonzero if the state ρ_h is non-passive, which can arise due to population inversion or thanks to certain coherences for example. Understanding the dynamical and steady state behaviours of the ergotropy \mathcal{E} for the bipartite quantum battery, with linear and quadratic drivings respectively, is the principle goal of this theoretical study.

For the purposes of the following calculations, it is convenient to work with the rotated density matrix $\rho \rightarrow \tilde{\rho}$, found via the transformation $\tilde{\rho} = e^{i\omega_a t(c^\dagger c + h^\dagger h)} \rho e^{-i\omega_a t(c^\dagger c + h^\dagger h)}$. This leads to the quantum master equation for $\tilde{\rho}$, complete with the effective Hamiltonian operator $\hat{\mathcal{H}}$, as follows [cf. Eqs. (2)–(5)]

$$\partial_t \tilde{\rho} = i[\tilde{\rho}, \hat{\mathcal{H}}] + \frac{\gamma}{2}\mathcal{L}_c[\tilde{\rho}], \tag{9}$$

$$\begin{aligned} \hat{\mathcal{H}} = & \Delta(c^\dagger c + h^\dagger h) + g(c^\dagger h + h^\dagger c) \\ & + \Omega(e^{i\theta} c^\dagger + e^{-i\theta} c), \end{aligned} \tag{10}$$

where we have introduced the driving-battery detuning frequency $\Delta = \omega_b - \omega_a$. The rotation of the reduced density matrix $\rho_h \rightarrow \tilde{\rho}_h$ is similarly governed by $\tilde{\rho}_h = e^{i\omega_a t h^\dagger h} \rho_h e^{-i\omega_a t h^\dagger h}$, such that the energies of interest [cf. Eq. (6) and Eq. (7)] can be equivalently written as $E_h = \text{Tr}\{\hat{H}_h \tilde{\rho}_h\}$ and $E_h^\beta = \text{Tr}\{\hat{H}_h \tilde{\rho}_h^\beta\}$. Furthermore, the

properties of traces and partial traces allows for the aforementioned energetic quantities, given in terms of the reduced density matrices $\tilde{\rho}_h$ and $\tilde{\rho}_h^\beta$, to be reconfigured in terms of the full (and rotated) density matrix $\tilde{\rho}$ like so: $\text{Tr}\{\hat{H}_h \tilde{\rho}_h\} = \text{Tr}\{\hat{H}_h \tilde{\rho}\}$ and $\text{Tr}\{\hat{H}_h \tilde{\rho}_h^\beta\} = \text{Tr}\{\hat{H}_h \tilde{\rho}^\beta\}$. Given this identification, one can use the trace property $\text{Tr}\{\mathcal{O}\tilde{\rho}\} = \langle \mathcal{O} \rangle$, which is valid for any operator \mathcal{O} , to simplify both energies of interest E_h and E_h^β . We consider the initial state of the system (at $t = 0$) to be the product of the local vacuum states of the battery charger and battery holder respectively, $\tilde{\rho}(t = 0) = |0\rangle\langle 0|_c \otimes |0\rangle\langle 0|_h$, after which both battery components start to interact as the charging process commences.

Pleasingly, one may exploit some neat properties of Gaussian systems^{46–48} in order to fully determine the passive state energy E_h^β (see Supplementary Note 1 and elsewhere⁵ for more details). We then finally arrive at compact expressions for both Eq. (6) and Eq. (7) in terms of operator expectation values, as follows

$$E_h = \omega_b \langle h^\dagger h \rangle, \tag{11}$$

$$E_h^\beta = \omega_b \left(\frac{\sqrt{\mathcal{D}} - 1}{2} \right). \tag{12}$$

Here we have introduced the dimensionless quantity \mathcal{D} , which collects the first and second moments of the battery holder, that is objects like $\langle h \rangle$ and $\langle h^\dagger h \rangle$, in the form

$$\mathcal{D} = \{1 + 2\langle h^\dagger h \rangle - 2\langle h^\dagger \rangle \langle h \rangle\}^2 - 4|\langle hh \rangle - \langle h \rangle|^2. \tag{13}$$

Now the ergotropy \mathcal{E} of the battery holder can be readily computed via Eq. (8), along with Eq. (11)–(13). In what follows, we consider the dynamical and steady state ergotropies for the composite quantum battery system, firstly with the one-photon driving case of Eq. (5) and then for the arguably more interesting quadratic case, featuring two-photon driving of the battery charger.

Linear quantum battery. The situation with one-photon coherent driving, as sketched in Fig. 1a and as governed by the Hamiltonian operator $\hat{\mathcal{H}}$ of Eq. (10), readily allows for analysis of the first and second moments (as is carried out in Supplementary Note 2, see also calculations in the literature⁵ for the more specific case with $\Delta = 0$). Since the system correlators factorise perfectly, such that $\langle h^\dagger h \rangle = \langle h^\dagger \rangle \langle h \rangle$ and $\langle hh \rangle = \langle h \rangle \langle h \rangle$ for example, the key quantity \mathcal{D} as defined in Eq. (13) simply reduces to

$$\mathcal{D} = 1. \tag{14}$$

This correlator factorisation stems from the joint battery charger–battery holder system evolving in a product state^{46–48}. (Notably, the neat Eq. (14) is not met when there is nonzero incoherent driving, which leads to unuseful energy storage in that particular case, as discussed previously⁵). Given the form of Eq. (14), the battery holder state must be pure due to the properties of Gaussian systems⁴⁸. Hence all of the stored energy in the battery holder is useful because the passive state energy must be [cf. Eq. (12)]

$$E_h^\beta = 0. \tag{15}$$

Therefore the ergotropy-to-battery-holder energy ratio for the linear quantum battery is, most pleasantly, a perfect one: $\mathcal{E}/E_h = 1$ [cf. Eq. (8)].

In the steady state ($t \rightarrow \infty$), the ergotropy \mathcal{E} , and identically the energy E_h of the battery holder, are simply given by [see Eq. (11)]

and Supplementary Note 2]

$$\lim_{t \rightarrow \infty} \mathcal{E} = \lim_{t \rightarrow \infty} E_h = \omega_b \frac{(g\Omega)^2}{(\Delta^2 - g^2)^2 + (\frac{\gamma}{2}\Delta)^2}. \quad (16)$$

Quite intuitively, maximising the steady state ergotropy \mathcal{E} requires the maximisation of the driving amplitude Ω and the minimisation of the charger decay rate γ . There is a more complicated competition between the charger-holder coupling strength g and the driving-battery detuning Δ . Typical circumstances are plotted in Fig. 1b, c, for example, cases with the couplings $g = \gamma$ and $g = \gamma/(2\sqrt{2}) \simeq 0.35\gamma$, respectively. In these two panels, the darker the colour the larger the steady state ergotropy \mathcal{E} , showcasing how the ergotropic maximum depends nontrivially on the detuning Δ . Denoting the specific value of the detuning Δ corresponding to the ergotropy maximum in the steady state as Δ' , one finds the relation

$$\Delta' = \sqrt{g^2 - \left(\frac{\gamma}{2\sqrt{2}}\right)^2} \Theta\left(g - \frac{\gamma}{2\sqrt{2}}\right), \quad (17)$$

where $\Theta(x)$ is the Heaviside step function. This formula suggests that zero detuning is optimal for smaller couplings $g \leq \gamma/(2\sqrt{2})$ below a critical value, while otherwise a nonzero detuning is preferable—as is hinted at in Fig. 1b, c and as shown explicitly in Fig. 1d. Inserting Eq. (17) into Eq. (16) yields the most desirable steady state ergotropies \mathcal{E} , depending upon the relative weightings between g and γ , as follows

$$\lim_{t \rightarrow \infty} \max\{\mathcal{E}\} = \begin{cases} \omega_b \left(\frac{\Omega}{g}\right)^2, & g \leq \frac{\gamma}{2\sqrt{2}}, \\ \omega_b \left(\frac{\Omega}{\gamma}\right)^2 \frac{(4g)^2}{(2g^2 - (\frac{\gamma}{2})^2)^2}, & g > \frac{\gamma}{2\sqrt{2}}, \end{cases} \quad (18)$$

as is plotted explicitly in Fig. 1e. Most notably, for smaller couplings $g \leq \gamma/(2\sqrt{2})$ there is a simple quadratic relation for the largest steady state ergotropy, as was discussed in detail previously⁵. For larger couplings $g \gg \gamma/(2\sqrt{2})$, the largest steady state ergotropy becomes independent of the coupling g as it tends towards $\lim_{t \rightarrow \infty} \mathcal{E} = \omega_b(2\Omega/\gamma)^2$, which features a natural competition between the drive amplitude Ω and the decay rate γ .

The time-dependent behaviour of this linear quantum battery is mainly determined by the complex eigenvalues ϵ_{\pm} , which arise from the dynamical matrix describing the first moments of the

system (see Supplementary Note 2), like so

$$\epsilon_{\pm} = \Delta \pm G - i\frac{\gamma}{4}, \quad \phi_{\pm} = \begin{pmatrix} 1 \\ \frac{g}{\epsilon_{\pm} - \Delta} \end{pmatrix}, \quad (19)$$

where ϕ_{\pm} are the associated eigenvectors. Here we have introduced the renormalized coupling strength G and (for use later on) a closely associated parameter known here as the renormalized decay rate Γ , which are defined together via

$$G = \sqrt{g^2 - \left(\frac{\gamma}{4}\right)^2}, \quad \Gamma = \sqrt{\left(\frac{\gamma}{4}\right)^2 - g^2}. \quad (20)$$

The real and imaginary parts of the complex eigenvalues ϵ_{\pm} are plotted in Fig. 2a, b using Eq. (19). Most interestingly when the coupling strength satisfies $g = g_{EP}$ (dashed and grey vertical lines in both panels), where

$$g_{EP} = \frac{\gamma}{4}, \quad (21)$$

the twin objects provided in Eq. (19) simultaneously coalesce, such that Eq. (21) highlights the presence of an exceptional point in the dynamical system. Exceptional points are known to be highly consequential in systems which may be described as non-Hermitian in some sense, and typically they mark the borderland between regimes with very different physical responses^{49–53}.

The dynamical ergotropy \mathcal{E} can be calculated using the framework built in Supplementary Note 2, and the analysis is most easily done for the case of zero drive-battery detuning ($\Delta = 0$). We start by noting that in the completely dissipationless battery charger limit (that is, when $\gamma \rightarrow 0$), one finds the oscillating ergotropy

$$\lim_{\gamma \rightarrow 0} \mathcal{E} = \omega_b \left(\frac{2\Omega}{g}\right)^2 \sin^4\left(\frac{gt}{2}\right), \quad (22)$$

which clearly reaches its maximum value of $\omega_b(2\Omega/g)^2$ at the time $t = \pi/g$ (and at all later times with the periodicity of $2\pi/g$). Within this lossless regime, we have also obtained the result equivalent to Eq. (22) but with the counter-rotating terms in the coupling Hamiltonian of Eq. (4) also included, which may be useful for future considerations of ultrastrongly coupled systems (see Supplementary Note 2). Otherwise, within the full driven-dissipative theory, there are two regimes of interest (split by an intermediate marginal case) due to the presence of the exceptional point of Eq. (21). These cases may be described

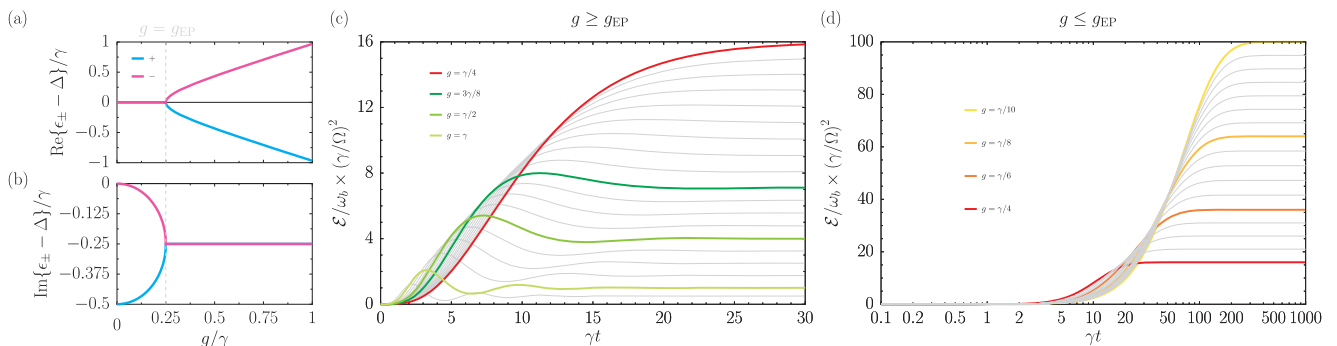


Fig. 2 The linear quantum battery and its dynamics. Panel **a**: the real parts of the complex eigenvalues ϵ_{\pm} , shifted by the drive-battery detuning Δ , as a function of the charger-holder coupling strength g (both in units of the charger damping rate γ) using Eq. (19). Panel **b**: as for panel **a**), but for the imaginary parts. Dashed grey lines: the exceptional point g_{EP} [cf. Eq. (21)]. Panel **c**: the ergotropy \mathcal{E} , scaled by $(\gamma/\Omega)^2$ and in units of ω_b , as a function of time t (in units of the inverse of γ). Thick coloured lines: the results for various values of the coupling g above the exceptional point ($g \geq g_{EP}$). Thin grey lines: intermediate couplings as guides for the eye. Panel **d**: as for panel **c**), but for couplings g below the exceptional point ($g \leq g_{EP}$), and plotted as a semi-logarithmic plot. In panels **(c)** and **(d)**, we consider the case of zero detuning ($\Delta = 0$), as governed by Eqs. (23)–(25).

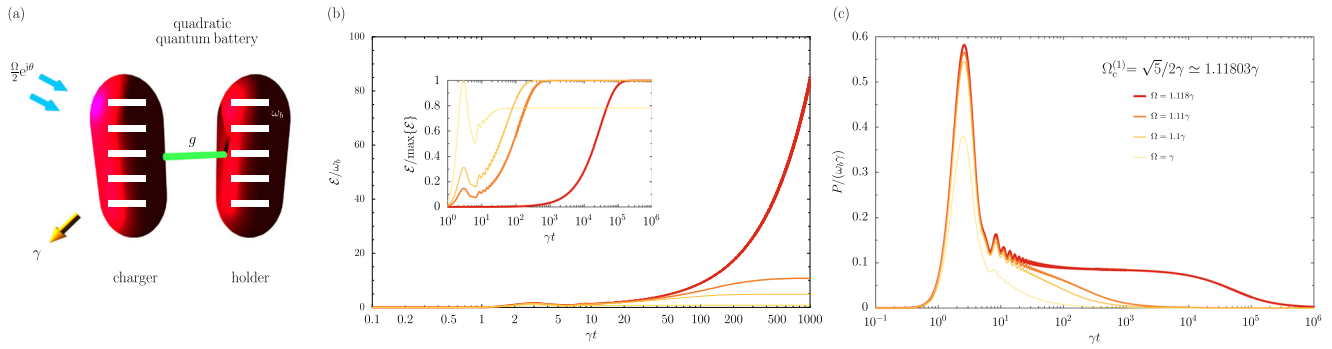


Fig. 3 The quadratic quantum battery and its dynamics. Panel **a**: a sketch of the bipartite quantum battery (both parts are modelled as harmonic oscillators, with the level spacing ω_b), composed of a battery charger coupled to a battery holder at the coupling strength g (green bar). The charger is driven parametrically (two cyan arrows) with an amplitude Ω , phase θ and frequency $2\omega_d$, while it suffers a loss (yellow arrow) at the decay rate γ . Panel **b**: a semi-logarithmic plot of the ergotropy \mathcal{E} (in units of ω_b) as a function of time t (in units of the inverse of γ) [cf. Eq. (11) and Eq. (12) with Eq. (44)]. Inset: as for panel **b**, but with the ergotropy \mathcal{E} scaled by its maximum value and with the timescale considered extended. Panel **c**: a semi-logarithmic plot of the power $P = \mathcal{E}/t$ (in units of $\omega_b\gamma$) as a function of time t . In panels **b** and **c**, we consider the case where $g = \gamma$ and $\Delta = \gamma/2$, so that from Eq. (40), the first critical driving amplitude $\Omega_c^{(1)} = \sqrt{5}/2\gamma \simeq 1.118\gamma$, while the second critical driving amplitude $\Omega_c^{(2)} = \sqrt{5/2}\gamma \simeq 1.581\gamma$ [cf. Eq. (41)]. The plot legend in panel **(c)** also applies to panel **(b)** and marks the various driving amplitudes Ω considered.

analytically with the expressions

$$\mathcal{E} = \omega_b \left(\frac{\Omega}{g}\right)^2 \left\{ 1 - \left[\cosh(\Gamma t) + \frac{\gamma}{4\Gamma} \sinh(\Gamma t) \right] e^{-\frac{\gamma}{4}t} \right\}^2, g < g_{EP}, \quad (23)$$

$$\mathcal{E} = \omega_b \left(\frac{4\Omega}{\gamma}\right)^2 \left\{ 1 - \left[1 + \frac{\gamma t}{4} \right] e^{-\frac{\gamma}{4}t} \right\}^2, g = g_{EP}, \quad (24)$$

$$\mathcal{E} = \omega_b \left(\frac{\Omega}{g}\right)^2 \left\{ 1 - \left[\cos(Gt) + \frac{\gamma}{4G} \sin(Gt) \right] e^{-\frac{\gamma}{4}t} \right\}^2, g > g_{EP}, \quad (25)$$

where the twin frequencies G and Γ are both defined in Eq. (20). Remarkably, the physics of the exceptional point ensures damped-hyperbolic, damped-algebraic and damped-trigonometric ergotropic behaviours are all possible, depending upon the relative strength of the charger-holder coupling g as compared to the charger decay rate γ . Notably, we always maintain the coupling regime $g \ll \omega_b$ within our driven-dissipative theory in order to avoid the discarded counter-rotating terms in the original Hamiltonian becoming non-negligible, as was discussed after Eq. (5). Nevertheless, in the extreme limiting cases of very weak ($g \ll \gamma$) and very strong ($g \gg \gamma$) couplings, as defined in comparison to the loss parameter γ only, the ergotropy \mathcal{E} follows the even simpler approximate expressions

$$\lim_{g \ll \gamma} \mathcal{E} \simeq \omega_b \left(\frac{\Omega}{g}\right)^2 \left\{ 1 - e^{-\left(\frac{\gamma}{4}-\Gamma\right)t} \right\}^2, \quad (26)$$

$$\lim_{g \gg \gamma} \mathcal{E} = \omega_b \left(\frac{\Omega}{g}\right)^2 \left\{ 1 - \cos(gt) e^{-\frac{\gamma}{4}t} \right\}^2. \quad (27)$$

With vanishing coupling g , the rough expression of Eq. (26) demonstrates the exponential rise in time of the ergotropy \mathcal{E} towards its eventual steady state value [cf. Eq. (16)]

$$\lim_{t \rightarrow \infty} \mathcal{E} = \omega_b \left(\frac{\Omega}{g}\right)^2, \quad (28)$$

as delicately controlled by the time constant $(\gamma/4 - \Gamma)^{-1}$ and its double within Eq. (26). The very strong coupling g result of Eq. (27) describes periodic oscillations, optimally bounded by 0 and $\omega_b(2\Omega/g)^2$, which are gradually damped out towards the

common steady state ergotropy of Eq. (28), which is notably at a value of one-quarter of its dynamical maximum.

The time-dependent ergotropy \mathcal{E} , for various couplings $g > g_{EP}$ above the exceptional point is shown in Fig. 2c using the exact result of Eq. (25). This panel displays Rabi-style oscillations (which are stronger with larger g) before an eventual decay into a steady state with a rather moderate ergotropy \mathcal{E} . The red line in panel (c) represents the border case, as governed by Eq. (24), where the coupling $g = g_{EP}$ exactly. For smaller couplings $g < g_{EP}$ below the exceptional point, the dynamics are similarly plotted in Fig. 2d using Eq. (23). Now Rabi-style oscillations are entirely absent, and the system instead monotonically increases in time towards a plateau at a much larger ergotropy \mathcal{E} [cf. Eq. (28)], albeit at the cost of much larger charging times. We have checked that the general physics of the linear quantum battery, including the interesting exceptional point physics, is maintained even after the inclusion of loss from the battery holder (see Supplementary Note 2).

Quadratic quantum battery. The perspectives for a highly ergotropic quantum battery can arguably be improved by instead considering parametric driving^{54–57}. The quadratic nature of the resultant Hamiltonian ensures that the ergotropy-to-battery holder energy ratio can be readily calculated using the same Gaussian theoretical framework as for the linear quantum battery [cf. Eqs. (11)–(13)], while the two-photon driving should lead to larger population inversions.

Let us replace the original driving Hamiltonian \hat{H}_d of Eq. (5) with a two-photon drive given by

$$\hat{H}_d = \frac{\Omega}{2} \left(e^{i\theta} e^{-2i\omega_d t} c^\dagger c^\dagger + e^{-i\theta} e^{2i\omega_d t} cc \right), \quad (29)$$

which nicely fits into the full Hamiltonian operator \hat{H} of Eq. (1). This quadratic quantum battery model is sketched in Fig. 3a, where the parametric drive is of amplitude $\Omega \geq 0$, phase θ and frequency $2\omega_d$. The analysis leading to the quantum master equation of Eq. (9) also holds for the quadratic driving case after the replacement of the effective Hamiltonian operator $\hat{\mathcal{H}}$ of Eq. (10) with

$$\hat{\mathcal{H}} = \Delta(c^\dagger c + h^\dagger h) + g(c^\dagger h + h^\dagger c) + \frac{\Omega}{2} e^{i\theta} c^\dagger c^\dagger + \frac{\Omega}{2} e^{-i\theta} cc. \quad (30)$$

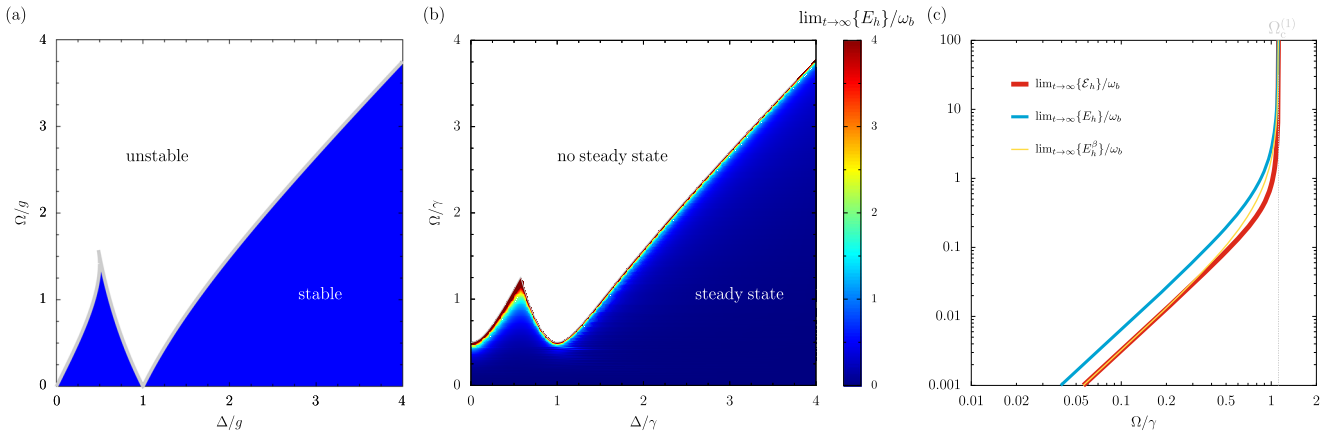


Fig. 4 The quadratic quantum battery and its phase diagram. Panel **a**: the Hamiltonian phase diagram of the quantum battery, as a function of the drive-battery detuning Δ and the two-photon driving amplitude Ω (both in units of the charger-holder coupling strength g). The stable (blue) region is associated with wholly real Hamiltonian eigenfrequencies ω_{\pm} , and the unstable (white) region corresponds to at least one complex eigenfrequency [cf. Eq. (32)]. Grey lines: boundaries coming from Eq. (36)–(38). Panel **b**: the Liouvillian phase diagram of the quantum battery in the steady state ($t \rightarrow \infty$), as a function of Δ and Ω (both in units of the charger damping rate γ). The white region corresponds to the situation where no steady state can be formed, while the coloured region describes when a steady state is established. The borders are given by Eq. (40) and Eq. (41). Colour bar: the battery holder energy E_h in the steady state (in units of the battery holder energy level spacing ω_b) from Eq. (39). In this panel, we consider the case of $g = \gamma$, and we cap the energy at the maximum value of $E_h = 4\omega_b$ in the colour bar. Panel **c**: a logarithmic plot of the salient steady state energies as a function of Ω (in units of γ). The ergotropy \mathcal{E} (thick red line) [cf. Eq. (8)], the battery holder energy E_h (medium cyan line) [cf. Eq. (39)], and the battery holder energy in the passive state E_h^β (thin yellow line) [cf. Eq. (12) with Eq. (45)] are all shown. Dashed grey line: the critical driving amplitude $\Omega_c^{(1)}$. In this panel, we consider $\Delta = \gamma/2$ and $g = \gamma$, so that $\Omega_c^{(1)} = \sqrt{5}\gamma/2 \simeq 1.118\gamma$ and $\Omega_c^{(2)} = \sqrt{5/2}\gamma \simeq 1.581\gamma$ from Eq. (40) and Eq. (41), respectively.

The two-photon driving appearing within Eq. (30) implies the presence of quantum squeezing⁵⁸, in stark contrast to the one-photon driving case described previously in Eqs. (2)–(5). The quadratic Hamiltonian operator $\hat{\mathcal{H}}$ provided in Eq. (30) may be diagonalized exactly by bosonic Bogoliubov transformation^{59,60} into the two-mode form

$$\hat{\mathcal{H}} = \sum_{\tau=\pm} \omega_{\tau} \beta_{\tau}^{\dagger} \beta_{\tau}, \quad (31)$$

where the mode index $\tau = \pm$ characterises the two Bogoliubov eigenfrequencies ω_{\pm} , as defined by the expression

$$\omega_{\pm} = \sqrt{\Delta^2 + g^2 - \frac{\Omega^2}{2} \pm \sqrt{\Omega^2 \left(\frac{\Omega^2}{4} - g^2 \right) + 4g^2 \Delta^2}}. \quad (32)$$

The twin Bogoliubov operators β_{\pm} appearing in Eq. (31) satisfy the standard bosonic commutation rule $[\beta_{\pm}, \beta_{\pm}^{\dagger}] = 1$, and they are composed of all four operators of the problem (c, h, c^{\dagger} , and h^{\dagger}) as follows

$$\beta_{\pm} = \frac{1}{\sqrt{2}} \begin{pmatrix} \cosh(\mu_{\pm}) \\ \cosh(\nu_{\pm}) \\ e^{i\theta} \sinh(\mu_{\pm}) \\ e^{i\theta} \sinh(\nu_{\pm}) \end{pmatrix}^T \cdot \begin{pmatrix} c \\ h \\ c^{\dagger} \\ h^{\dagger} \end{pmatrix}, \quad (33)$$

where the Bogoliubov coefficients in Eq. (33) may be found from the hyperbolic tangent relations

$$\tanh(\mu_{\pm}) = \frac{\Omega(\Delta + \omega_{\pm})}{(\Delta + \omega_{\pm})^2 - g^2}, \quad (34)$$

$$\tanh(\nu_{\pm}) = \frac{\Omega(\Delta - \omega_{\pm})}{(\Delta + \omega_{\pm})^2 - g^2}. \quad (35)$$

We also note that inverting the operators of Eq. (33) allows for the nontrivial vacuum state populations of the battery charger and battery holder to be calculated (see Supplementary Note 3), while

the squeezing promised by the counter-rotating driving terms is considered later on. Most interestingly, the two Bogoliubov eigenfrequencies ω_{\pm} of Eq. (32) are not wholly real for all values of the three Hamiltonian parameters Δ, Ω and g . This suggests a spectral collapse^{61,62} within the purely Hamiltonian theory of Eq. (30) in certain parameter regimes. The phase diagram implied by the stability of the solely Hamiltonian operator $\hat{\mathcal{H}}$ approach is plotted in Fig. 4a, where the boundaries (grey lines) are defined by the three equations [cf. when Eq. (32) become complex]

$$\Omega = \left| \Delta - \frac{g^2}{\Delta} \right| \Theta \left(\frac{\Delta}{g} - \Xi \right), \quad (36)$$

$$\Omega = g \left(\sqrt{1 + 2\frac{\Delta}{g}} - \sqrt{1 - 2\frac{\Delta}{g}} \right) \Theta \left(\frac{1}{2} - \frac{\Delta}{g} \right), \quad (37)$$

$$\Omega = g \left(\sqrt{1 + 2\frac{\Delta}{g}} + \sqrt{1 - 2\frac{\Delta}{g}} \right) \Theta \left(\frac{1}{2} - \frac{\Delta}{g} \right) \Theta \left(\frac{\Delta}{g} - \Xi \right), \quad (38)$$

where the dimensionless number $\Xi = \sqrt{\sqrt{5} - 2} \simeq 0.486$. The diagram of Fig. 4a hints at a classification where the stable regions (blue, real ω_{\pm}) are associated with convergent-in-time dynamics, while the unstable regions (white, complex ω_{\pm}) should not be able to support a steady state due to their divergent-in-time dynamics. The introduction of dissipation into the system via the quantum master equation of Eq. (9) upgrades the simple Hamiltonian dynamics of Eq. (31) and necessarily updates the phase diagram of Fig. 4a in a more physically meaningful manner (for example, the imaginary parts of complex eigenfrequencies can then be interpreted as being related to inverse lifetimes), as we now explore with proper reference to the steady state of the full driven-dissipative system.

Within an open quantum systems approach, the steady state energy of the battery holder E_h [cf. Eq. (11)] may be found from the first and second moments of the system (see Supplementary

Note 3 for the full theory). This leads to the analytic expression

$$\lim_{t \rightarrow \infty} E_h = \omega_b \frac{\Omega^2}{(2\Delta)^2 + \left(\frac{\gamma}{2}\right)^2 - \Omega^2} \frac{\Delta^4 + \frac{g^4}{2} - \Delta^2 \left[\frac{g^2}{2} + \Omega^2 - \left(\frac{\gamma}{2}\right)^2 \right]}{\Delta^4 + g^4 - \Delta^2 \left[2g^2 + \Omega^2 - \left(\frac{\gamma}{2}\right)^2 \right]}, \quad (39)$$

which may be compared to Eq. (16), the analogous result with one-photon driving. Notably, the denominators of both the first and second terms in the product of fractions comprising Eq. (39) may each become zero at some point in parameter space, suggesting two critical driving amplitudes of the system—which we call $\Omega_c^{(1)}$ and $\Omega_c^{(2)}$. These critical points are given by [cf. Eq. (36)–(38) from the Hamiltonian theory]

$$\Omega_c^{(1)} = \sqrt{\left(\frac{\gamma}{2}\right)^2 + (2\Delta)^2}, \quad (40)$$

$$\Omega_c^{(2)} = \sqrt{\left(\frac{\gamma}{2}\right)^2 + \Delta^2 \left(1 - \frac{g^2}{\Delta^2}\right)^2}, \quad (41)$$

and help to define the Liouvillian phase diagram of the quadratic quantum battery in the steady state via the duo of equations $\Omega = \Omega_c^{(1)} \Theta(1/\sqrt{3} - \Delta/g)$ and $\Omega = \Omega_c^{(2)} \Theta(\Delta/g - 1/\sqrt{3})$. The steady-state battery holder energy E_h is plotted in Fig. 4b, where the situation without a steady state is represented by the white region. Clearly, approaching the critical line formed using Eq. (40) and Eq. (41) leads to a transition in the steady state response of the quantum battery—above this dynamical instability, the energetics are unbounded since the mean battery populations are themselves unbounded. This is because the energetic drive into the battery more than compensates for the loss into the external environment, leading to a dramatic rise of bosonic excitations up the infinite energy ladders comprising the quadratic quantum battery. The energy formula of Eq. (39) becomes much simpler in the two limiting cases of small detuning ($\Delta \rightarrow 0$) and small battery charger-holder coupling ($g \rightarrow 0$), where

$$\lim_{t \rightarrow \infty} E_h = \frac{\omega_b}{2} \frac{\Omega^2}{\left(\frac{\gamma}{2}\right)^2 - \Omega^2}, \quad \Delta \rightarrow 0, \quad (42)$$

$$\lim_{t \rightarrow \infty} E_h = \omega_b \frac{\Omega^2}{(2\Delta)^2 + \left(\frac{\gamma}{2}\right)^2 - \Omega^2}, \quad g \rightarrow 0. \quad (43)$$

The left-hand vertical axis of Fig. 4b is explained by Eq. (42), complete with its finishing point at $\Omega = \gamma/2$, above which no steady state is formed. Meanwhile, Eq. (43) describes the weakly coupled battery result (not shown in Fig. 4b, which takes $g = \gamma$ as an example case), which sees a reduction in the number of critical points from two to one, located at $\Omega_c^{(1)}$ only [cf. Eq. (40)]. The phase diagram of Fig. 4b illustrates the critical nature of the quadratic quantum battery, where significant energies can be obtained near dynamical instabilities governed by critical points, which may be starkly contrasted to the linear quantum battery, which is instead dominated by exceptional point physics.

The quadratic nature of the Hamiltonian operator $\hat{\mathcal{H}}$ given by Eq. (30) ensures that the result of Eq. (12), quantifying the energy of the battery holder in the passive state E_h^β , also holds. In particular, the initial conditions of the system imply that the first moments of the system are all zero (see Supplementary Note 3 for details). Therefore the key quantity \mathcal{D} , as defined in Eq. (13), reduces to the solely second moments form [cf. Eq. (15) for the linear quantum battery]

$$\mathcal{D} = (1 + 2\langle h^\dagger h \rangle)^2 - 4\langle h^\dagger h^\dagger \rangle \langle h h \rangle. \quad (44)$$

Notably, since, in general, $\mathcal{D} \neq 1$ the quadratic quantum battery is associated with nonzero passive state energy ($E_h^\beta \neq 0$), which acts to reduce the ergotropy \mathcal{E} following the definition of Eq. (8). In the crucial steady-state regime ($t \rightarrow \infty$), the explicit form of Eq. (44) is derivable exactly as (see Supplementary Note 3)

$$\lim_{t \rightarrow \infty} \mathcal{D} = \frac{\left[(2\Delta)^2 + \left(\frac{\gamma}{2}\right)^2 \right]^2 \left[(\Delta^2 - g^2)^2 + \Delta^2 \left(\frac{\gamma}{2}\right)^2 \right] - \Omega^2 \left[(2\Delta)^2 + \left(\frac{\gamma}{2}\right)^2 \right] \left[2\Delta^4 + g^4 - \Delta^2 \left(2g^2 + \left(\frac{\gamma}{2}\right)^2 \right) \right] - \Delta^2 \Omega^4 \left[7\Delta^2 - 4g^2 + \left(\frac{\gamma}{2}\right)^2 \right] - \Delta^2 \Omega^6}{\left[(2\Delta)^2 + \left(\frac{\gamma}{2}\right)^2 - \Omega^2 \right]^2 \left[\Delta^4 - \Delta^2 \left[2g^2 + \Omega^2 - \left(\frac{\gamma}{2}\right)^2 \right] + g^4 \right]}. \quad (45)$$

This analytic result ensures that the steady state ergotropy \mathcal{E} has been analytically obtained with the aid of the analytic expression of the holder energy E_h [cf. Eq. (39)] alongside the exact passive state holder energy E_h^β [cf. Eq. (12) with Eq. (45)]. The full expression for the steady state ergotropy \mathcal{E} is particularly compact in the limiting case of small detuning ($\Delta \rightarrow 0$), where we find it reduces to

$$\lim_{t \rightarrow \infty} \mathcal{E} = \frac{\omega_b}{2} \left(\frac{\left(\frac{\gamma}{2}\right)^2}{\left(\frac{\gamma}{2}\right)^2 - \Omega^2} - \sqrt{\frac{\left(\frac{\gamma}{2}\right)^2}{\left(\frac{\gamma}{2}\right)^2 - \Omega^2}} \right), \quad (46)$$

which exhibits a single critical point at $\Omega_c^{(1)} = \gamma/2$ [cf. Eq. (40)]. In the limit of small charger-holder coupling g , one finds that the full expression reduces to the intuitive result of zero steady-state ergotropy ($\lim_{t \rightarrow \infty} \mathcal{E} = 0$ for the case of $g \rightarrow 0$).

We consider the steady state energetics of the quadratic quantum battery in Fig. 4c, as a function of the driving amplitude Ω , for the example case where the detuning $\Delta = \gamma/2$ and the charger-holder coupling $g = \gamma$. The ergotropy \mathcal{E} (thick red line) [cf. Eq. (8)], the battery holder energy E_h (medium cyan line) [cf. Eq. (39)], and the battery holder energy in the passive state E_h^β (thin yellow line) [cf. Eq. (12) with Eq. (45)] are all shown explicitly in their steady-state forms. As the driving amplitude, Ω approaches the critical point at $\Omega_c^{(1)} = \sqrt{5/2}\gamma \simeq 1.118\gamma$ (dashed grey line) [cf. Eq. (40)] all three energetic quantities increase without bound, leading to an abundance of useful energy being stored in the battery. This boundlessness occurs since a steady state is no longer supportable within this driven-dissipative theory when the drive into the battery overcompensates the loss into the outside environment. In practice, such a seemingly runaway solution may be prevented by either truncating the infinite energy ladders associated with the harmonic oscillators forming the quantum battery model, leading instead to saturation at some large energy (as is discussed later on), or by introducing anharmonicities. Importantly, there are no analogous critical points in the linear quantum battery, and hence there is no such optimal driving associated with a huge ergotropic response.

The time-dependent properties of the ergotropy \mathcal{E} are considered in Fig. 3b. There we again take the example quadratic quantum battery with the charger-holder coupling $g = \gamma$ and the

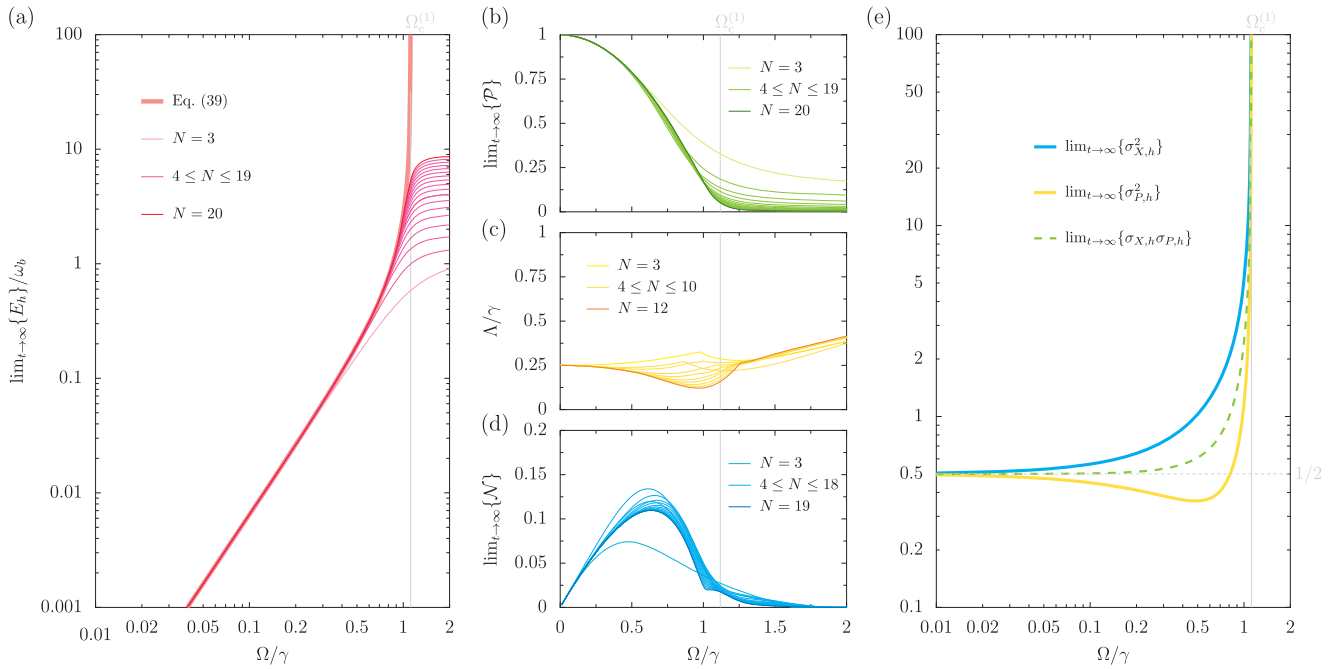


Fig. 5 The quadratic quantum battery and its steady state. Panel **a**: a logarithmic plot of the battery holder energy E_h in the steady state (in units of the holder energy level spacing ω_b) as a function of the two-photon driving amplitude Ω (in units of the charger decay rate γ). Thick line: the analytic result of Eq. (39). Thin lines: results obtained by truncating the harmonic oscillators modelling the battery to N -level systems. Panel **b**: the purity \mathcal{P} , in the steady state and as a function of Ω , for a battery comprised of N -level systems. Panel **c**: the Liouvillian gap Λ as a function of Ω . Panel **d**: the negativity \mathcal{N} , in the steady state and as a function of Ω . Panel **e**: a logarithmic plot of the battery holder quadrature variances $\sigma_{X,h}^2$ (thick cyan line) and $\sigma_{P,h}^2$ (thick yellow line) in the steady state and as a function of Ω . The product of the standard deviations $\sigma_{X,h}\sigma_{P,h}$ (medium dashed green line) is also shown as a guide for the eye at the Robertson-Schrödinger minimum uncertainty of $1/2$ (horizontal, dashed grey line). In the figure, the charger-holder coupling strength $g = \gamma$ and the drive-battery detuning $\Delta = \gamma/2$, so that from Eq. (40), the first critical driving amplitude $\Omega_c^{(1)} = \sqrt{5}\gamma/2 \simeq 1.118\gamma$ (vertical, solid grey lines in all panels).

detuning $\Delta = \gamma/2$, so that from Eq. (40), the first critical driving amplitude is $\Omega_c^{(1)} \simeq 1.118\gamma$, while the second critical driving amplitude from Eq. (41) is $\Omega_c^{(2)} \simeq 1.581\gamma$. Increasingly strong driving amplitudes Ω are considered up to $\Omega_c^{(1)}$ [see the plot legend in Fig. 3c for the cases considered], leading to dramatic ergotropic improvements at larger timescales $\gamma t \gg 1$, as foreshadowed by the steady state analysis provided in Fig. 4c. The inset of Fig. 3(b) rescales the ergotropy \mathcal{E} by its maximum value over all times, showing the typical timescales required for the battery to become fully charged (in an ergotropic sense). Notably, full charging is achieved asymptotically ($t \rightarrow \infty$) except for when the driving amplitude is furthest away (thin yellow line) from $\Omega_c^{(1)}$, where a dynamical ergotropic value is higher than its steady state value [a circumstance which commonly occurs for the linear quantum battery, see Fig. 2c]. Finally, the equivalent charging powers $P = \mathcal{E}/t$ for the ergotropies considered in Fig. 3b are shown in Fig. 3c. This panel c shows that the power P increases with time from zero up to some maximum power, which is seen to occur around the optimal time $t \simeq 2.6/\gamma$ for the cases considered. Hence the maximum power does not correspond to when the battery is fully charged [in the sense of the inset to Fig. 3b]. A logarithmic timescale is used in Fig. 3c to confirm the eventual loss of power when the steady state ergotropy is finally reached at large timescales. Notably, we have made sure that the general physics of the quadratic quantum battery, as described in Fig. 3 and Fig. 4 in particular, is essentially unchanged after including additional dissipation coming from the battery holder itself (see Supplementary Note 3).

The steady-state properties of the quadratic quantum battery are further considered in Fig. 5. In the figure, the charger-holder coupling strength remains at $g = \gamma$, and the drive-battery

detuning remains at $\Delta = \gamma/2$ so that the critical point $\Omega_c^{(1)} \simeq 1.118\gamma$ (vertical, solid grey lines in all panels of Fig. 5). In particular, we are interested in the results obtained by truncating the two harmonic oscillators modelling the battery charger and the battery holder to finite N -level systems, in order to better understand where the energetic unboundedness suggested in Fig. 4c arises from.

In Fig. 5a, we consider the battery holder energy E_h in the steady state (in units of the battery energy level spacing ω_b) as a function of the two-photon driving amplitude Ω (in units of the charger decay rate γ). The analytic (and $N \rightarrow \infty$ asymptotic) result of Eq. (39) is represented by the thick salmon-pink line, showcasing the aforementioned unboundedness as $\Omega \rightarrow \Omega_c^{(1)}$. Otherwise, the truncated oscillator results are denoted by thin pink lines (the extreme cases for $N=3$ and $N=20$ levels are distinguished with light pink and red lines, respectively). The data in Fig. 5a confirms the increasing impact of the first critical driving amplitude $\Omega_c^{(1)}$ with an increasing number of levels N and highlights the eventual plateauing of the battery holder energy E_h due to the necessary saturation of the finite level systems making up the truncated battery. These results support the main findings presented in Fig. 4c for infinite-level quantum harmonic oscillators and imply that the energetic unboundedness is a result of always being able to occupy higher and higher levels of an untruncated harmonic oscillator, as opposed to occurring due to an unphysical runaway or some unreasonable approximation.

The behaviour of the purity \mathcal{P} of the quadratic quantum battery, a measure of the degree of mixedness of the quantum state ρ via the formula $\mathcal{P} = \text{Tr}(\rho^2)$, is likewise shown in Fig. 5b for the steady state. The purity is bounded by $\mathcal{P} = 1$ for a pure state and $\mathcal{P} = 1/d$ (where d is the dimension of the relevant

Hilbert space) for a maximally mixed state. With vanishing driving Ω , the system remains in its vacuum state and is hence completely pure. However, for non-vanishing driving Ω the key quantity \mathcal{D} [cf. Eq. (13)] is non-unity, and the degree of mixedness rapidly increases as the driving amplitude Ω is increased towards the critical point $\Omega_c^{(1)}$, eventually leading to a maximally mixed quantum state and significant loss of coherences. This impure behaviour is in stark contrast to the completely pure linear quantum battery, which remains in a product state such that it exhibits the property $\mathcal{D} = 1$.

The underlying nature of the critical driving amplitude $\Omega_c^{(1)}$ can be revealed by considering the response of the Liouvillian gap Λ . This important quantity is defined as the gap between zero and the real part of the largest (nonzero) eigenvalue in the Liouvillian superoperator spectrum^{63–65}, and is displayed in Fig. 5c. The closing of the Liouvillian gap (which is possible in the true thermodynamic limit, where $N \rightarrow \infty$) at some critical value of a system parameter is typically associated with a dissipative phase transition^{66–68}. In the case of the quadratic quantum battery, the crucial parameter again seems to be the critical driving amplitude $\Omega_c^{(1)}$ (more evidence supporting this conjecture is provided in Supplementary Note 3, which suggests an algebraic scaling of the Liouvillian gap size with the system size N). No such closing of the Liouvillian gap is possible for the one-photon driving case considered previously for the linear quantum battery since, in that case, there is always a well-defined steady state [cf. Eq. (16) with Eq. (39)], and as such, no dynamical instability is present.

The fact that the key quantity $\mathcal{D} \neq 1$ [cf. Eq. (13)] for the quadratic quantum battery raises the possibility that quantum entanglement is playing a role. To investigate this, we consider the negativity \mathcal{N} , a common entanglement measure defined using the absolute sum of the negative eigenvalues of the partial transpose of the density matrix ρ ^{69,70}. Zero negativity implies an unentangled state, while increasingly nonzero negativity suggests an increasingly entangled state. We plot the negativity \mathcal{N} , again in the steady state and as a function of the driving amplitude Ω , in Fig. 5d. The plot shows that the state is completely unentangled with vanishing driving $\Omega \rightarrow 0$ since it is simply the trivial vacuum state. However, with increasingly strong driving Ω the entanglement of the state rises to a certain maximum before falling once again towards zero (in the thermodynamic $N \rightarrow \infty$ limit) near the critical point $\Omega_c^{(1)}$. This trend occurs since, for any truncated oscillator case, the state at some large enough driving Ω is simply that with the highest level filled. This type of entanglement behaviour is entirely missing in the linear quantum battery, which always remains in an unentangled product state.

Finally, the phenomena of quantum squeezing within the quadratic quantum battery may be analysed through the two battery holder quadrature variances $\sigma_{X,h}^2$ and $\sigma_{P,h}^2$ ⁵⁸. These dimensionless quantities, defined via the twin relations of $\sigma_{X,h}^2 = \langle \hat{X}_h^2 \rangle - \langle \hat{X}_h \rangle^2$ (thick cyan line) and $\sigma_{P,h}^2 = \langle \hat{P}_h^2 \rangle - \langle \hat{P}_h \rangle^2$ (thick yellow line), are considered (in the steady state and as a function of the driving amplitude Ω) in Fig. 5e. These variance definitions rely on the generalised battery holder quadratures $\hat{X}_h = (e^{i\theta/2} \hat{h}^\dagger + e^{-i\theta/2} \hat{h})/\sqrt{2}$ and $\hat{P}_h = i(e^{i\theta/2} \hat{h}^\dagger - e^{-i\theta/2} \hat{h})/\sqrt{2}$, which obey the familiar commutation relation $[\hat{X}_h, \hat{P}_h] = i$. The product of the standard deviations $\sigma_{X,h} \sigma_{P,h}$ (medium dashed green line) is also shown in Fig. 5e, as is a guide for the eye at the Robertson–Schrodinger minimum uncertainty of 1/2 (horizontal, dashed grey line). Most notably, the quasi-momentum variance $\sigma_{P,h}^2$ displays steady state squeezing for a range of driving amplitudes Ω , up to a certain value $\Omega \simeq 0.813\gamma$ (which is notably below the critical point residing at $\Omega_c^{(1)} \simeq 1.118\gamma$). Such

quadrature squeezing of the quadratic quantum battery directly originates from the parametric field driving and thus is entirely absent for the coherent field driving case of the linear quantum battery. Squeezing may be interesting for modern applications in quantum sensing and for quantum information processing, while here, it is interesting to note that the quadrature variances display asymptotes at $\Omega_c^{(1)}$, the onset of the dynamical instability discussed earlier. Within wider quantum battery research, squeezing has been recently studied in the context of a coherent squeezing charging mechanism and an incoherent squeezed thermal bath⁷¹, as well as battery charging with local squeezing⁷², which points to its utility within quantum technological research.

Conclusion

In conclusion, we have studied theoretically the prototypical bipartite form of a Gaussian quantum battery. We began by revisiting the case of a linearly driven battery charger, where we highlighted the crucial role of exceptional point physics in the ergotropic response of the battery. We then considered the arguably more interesting case of quadratic driving, where we found critical points instead play a decisive role in the battery energetics, including by influencing several unconventional features such as the spectral collapse of the Hamiltonian, quantum squeezing, dynamic instabilities and dissipative phase transitions. Our proposed quadratic quantum battery exhibits various desirable features, including storing only relatively small amounts of useless energy, allowing for the possibility of storing (theoretically unbounded) amounts of ergotropy, and requiring reasonable charging times to achieve significant energy storage. We hope that our theoretical proposal for a quadratic quantum battery can soon be realised with contemporary quantum platforms such as photonic cavities^{73,74} and quantum circuits^{75,76}, so that a squeezed battery may become a viable candidate for an energy storage device within the next generation of quantum technology. On the theory side, it should also be interesting to consider the scaling up of the quadratic quantum battery to include multiple battery cells^{77,78} and cooperative effects^{79,80}.

Data availability

All data is available in the manuscript and the Supplementary Information.

Received: 22 June 2023; Accepted: 23 October 2023;

Published online: 04 November 2023

References

- Kosloff, R. & Levy, A. Quantum heat engines and refrigerators: continuous devices. *Annu. Rev. Phys. Chem.* **65**, 365 (2014).
- Bhattacharjee, S. & Dutta, A. Quantum thermal machines and batteries. *Eur. Phys. J. B* **94**, 239 (2021).
- Alicki, R. & Fannes, M. Entanglement boost for extractable work from ensembles of quantum batteries. *Phys. Rev. E* **87**, 042123 (2013).
- For a review on quantum batteries, see: Campaioli, F., Gherardini, S., Quach, J. Q., Polini, M. & Andolina, G. M. Colloquium: quantum batteries. <https://arxiv.org/abs/2308.02277>.
- Farina, D., Andolina, G. M., Mari, A., Polini, M. & Giovannetti, V. Charger-mediated energy transfer for quantum batteries: an open-system approach. *Phys. Rev. B* **99**, 035421 (2019).
- Ferraro, D., Campisi, M., Andolina, G. M., Pellegrini, V. & Polini, M. High-power collective charging of a solid-state quantum battery. *Phys. Rev. Lett.* **120**, 117702 (2018).
- Andolina, G. M. et al. Charger-mediated energy transfer in exactly solvable models for quantum batteries. *Phys. Rev. B* **98**, 205423 (2018).
- Le, T. P., Levinsen, J., Modi, K., Parish, M. M. & Pollock, F. A. Spin-chain model of a many-body quantum battery. *Phys. Rev. A* **97**, 022106 (2018).

9. Barra, F. Dissipative charging of a quantum battery. *Phys. Rev. Lett.* **122**, 210601 (2019).
10. Zhang, Y.-Y., Yang, T.-R., Fu, L. & Wang, X. Powerful harmonic charging in a quantum battery. *Phys. Rev. E* **99**, 052106 (2019).
11. Santos, A. C., Cakmak, B., Campbell, S. & Zinner, N. T. Stable adiabatic quantum batteries. *Phys. Rev. E* **100**, 032107 (2019).
12. Pirmoradian, F. & Molmer, K. Aging of a quantum battery. *Phys. Rev. A* **100**, 043833 (2019).
13. Andolina, G. M. et al. Extractable work, the role of correlations, and asymptotic freedom in quantum batteries. *Phys. Rev. Lett.* **122**, 047702 (2019).
14. Crescente, A., Carrega, M., Sassetti, M. & Ferraro, D. Ultrafast charging in a two-photon Dicke quantum battery. *Phys. Rev. B* **102**, 245407 (2020).
15. Santos, A. C., Saguia, A. & Sarandy, M. S. Stable and charge-switchable quantum batteries. *Phys. Rev. E* **101**, 062114 (2020).
16. Carrega, M., Crescente, A., Ferraro, D. & Sassetti, M. Dissipative dynamics of an open quantum battery. *New J. Phys.* **22**, 083085 (2020).
17. Santos, A. C. Quantum advantage of two-level batteries in the self-discharging process. *Phys. Rev. E* **103**, 042118 (2021).
18. Xu, K., Zhu, H.-J., Zhang, G.-F. & Liu, W.-M. Enhancing the performance of an open quantum battery via environment engineering. *Phys. Rev. E* **104**, 064143 (2021).
19. Dou, F.-Q., Lu, Y.-Q., Wang, Y.-J. & Sun, J.-A. Extended Dicke quantum battery with interatomic interactions and driving field. *Phys. Rev. B* **105**, 115405 (2022).
20. Barra, F., Hovhannisyan, K. V. & Imparato, A. Quantum batteries at the verge of a phase transition. *New J. Phys.* **24**, 015003 (2022).
21. Carrasco, J., Maze, J. R., Hermann-Avigliano, C. & Barra, F. Collective enhancement in dissipative quantum batteries. *Phys. Rev. E* **105**, 064119 (2022).
22. Shi, H.-L., Ding, S., Wan, Q.-K., Wang, X.-H. & Yang, W.-L. Entanglement, coherence, and extractable work in quantum batteries. *Phys. Rev. Lett.* **129**, 130602 (2022).
23. Santos, T. F. F., Vianna de Almeida, Y. & Santos, M. F. Vacuum-enhanced charging of a quantum battery. *Phys. Rev. A* **107**, 032203 (2023).
24. Quach, J. Q. et al. Superabsorption in an organic microcavity: toward a quantum battery. *Sci. Adv.* **8**, eabk3160 (2022).
25. Joshi, J. & Mahesh, T. S. Experimental investigation of a quantum battery using star-topology NMR spin systems. *Phys. Rev. A* **106**, 042601 (2022).
26. Hu, C.-K. et al. Optimal charging of a superconducting quantum battery. *Quantum Sci. Technol.* **7**, 045018 (2022).
27. de Buy Wenniger, I. M. et al. Experimental analysis of energy transfers between a quantum emitter and light fields. <https://arxiv.org/abs/2202.01109>.
28. Cimini, V. et al. Experimental characterization of the energetics of quantum logic gates. *npj Quantum Inf.* **6**, 96 (2020).
29. Stevens, J. et al. Energetics of a single qubit gate. *Phys. Rev. Lett.* **129**, 110601 (2022).
30. Peterson, J. P. S. et al. Experimental characterization of a spin quantum heat engine. *Phys. Rev. Lett.* **123**, 240601 (2019).
31. Leghtas, Z. et al. Confining the state of light to a quantum manifold by engineered two-photon loss. *Science* **347**, 853 (2015).
32. Wang, C. et al. A Schrödinger cat living in two boxes. *Science* **352**, 1087 (2016).
33. Wang, Z. et al. Quantum dynamics of a few-photon parametric oscillator. *Phys. Rev. X* **9**, 021049 (2019).
34. Wustmann, W. & Shumeiko, V. Parametric effects in circuit quantum electrodynamics. *Low Temp. Phys.* **45**, 848 (2019).
35. Gaikwad, C., Kowsari, D., Chen, W. & Murch, K. W. Observing parity time symmetry breaking in a Josephson parametric amplifier. <https://arxiv.org/abs/2306.14980>.
36. Forn-Diaz, P., Lamata, L., Rico, E., Kono, J. & Solano, E. Ultrastrong coupling regimes of light-matter interaction. *Rev. Mod. Phys.* **91**, 025005 (2019).
37. Le Boite, A. Theoretical methods for ultrastrong light-matter interactions. *Adv. Quantum Technol.* **3**, 1900140 (2020).
38. Downing, C. A. & Toghiani, A. J. Quantum topology in the ultrastrong coupling regime. *Sci. Rep.* **12**, 11630 (2022).
39. Shaghghi, V., Singh, V., Benenti, G. & Rosa, D. Micromasers as quantum batteries. *Quantum Sci. Technol.* **7**, 04LT01 (2022).
40. Breuer, H.-P. & Petruccione, F. *The Theory of Open Quantum Systems* (Oxford University Press, Oxford, 2002).
41. Downing, C. A. & Sturges, T. J. Directionality between driven-dissipative resonators. *EPL* **140**, 35001 (2022).
42. Pusz, W. & Woronowicz, S. L. Maximal work extraction from finite quantum systems. *Commun. Math. Phys.* **58**, 273 (1977).
43. Lenard, A. Thermodynamical proof of the Gibbs formula for elementary quantum systems. *J. Stat. Phys.* **19**, 575 (1978).
44. Friis, N. & Huber, M. Precision and work fluctuations in Gaussian battery charging. *Quantum* **2**, 61 (2018).
45. Allahverdyan, A. E., Balian, R. & Nieuwenhuizen, T. M. Maximal work extraction from finite quantum systems. *Europhys. Lett.* **67**, 565 (2004).
46. Ferraro, A., Olivares, S. & Paris, M. *Gaussian States in Quantum Information* (Bibliopolis, Napoli, 2005). See also: <https://doi.org/10.48550/arXiv.quant-ph/0503237>.
47. Olivares, S. Quantum optics in the phase space. *Eur. Phys. J. Spec. Top.* **203**, 3 (2012).
48. Serafini, A. *Quantum Continuous Variables* (CRC Press, Boca Raton, 2017).
49. Berry, M. V. Physics of nonhermitian degeneracies. *Czech. J. Phys.* **54**, 1039 (2004).
50. Heiss, W. D. Exceptional points—their universal occurrence and their physical significance. *Czech. J. Phys.* **54**, 1091 (2004).
51. Ozdemir, S. K., Rotter, S., Nori, F. & Yang, L. Parity-time symmetry and exceptional points in photonics. *Nat. Mater.* **18**, 783 (2019).
52. Miri, M.-A. & Alu, A. Exceptional points in optics and photonics. *Science* **363**, 6422 (2019).
53. Downing, C. A. & Saroka, V. A. Exceptional points in oligomer chains. *Commun. Phys.* **4**, 254 (2021).
54. Minganti, F., Bartolo, N., Lollì, J., Casteels, W. & Ciuti, C. Exact results for Schrödinger cats in driven-dissipative systems and their feedback control. *Sci. Rep.* **6**, 26987 (2016).
55. Puri, S., Boutin, S. & Blais, A. Engineering the quantum states of light in a Kerr-nonlinear resonator by two-photon driving. *npj Quantum Inf.* **3**, 18 (2017).
56. Di Candia, R., Minganti, F., Petrovni, K. V., Paroanu, G. S. & Felicetti, S. Critical parametric quantum sensing. *npj Quantum Inf.* **9**, 23 (2023).
57. Downing, C. A. & Vidiella-Barranco, A. Parametrically driving a quantum oscillator into exceptionality. *Sci. Rep.* **13**, 11004 (2023).
58. Loudon, R. & Knight, P. L. Squeezed light. *J. Mod. Opt.* **34**, 709 (1987).
59. Tsallis, C. Diagonalization methods for the general bilinear Hamiltonian of an assembly of bosons. *J. Math. Phys.* **19**, 277 (1978).
60. Colpa, J. H. P. Diagonalization of the quadratic boson Hamiltonian. *Phys. A* **93**, 327 (1978).
61. Kirtou, P., Roses, M. M., Keeling, J. & Dalla Torre, E. G. Introduction to the Dicke Model: from equilibrium to nonequilibrium, and vice versa. *Adv. Quantum Technol.* **2**, 1800043 (2018).
62. Salado-Mejía, M., Román-Ancheyta, R., Soto-Eguibar, F. & Moya, H. M. Spectroscopy and critical quantum thermometry in the ultrastrong coupling regime. *Quantum Sci. Technol.* **6**, 025010 (2021).
63. Kessler, E. M. et al. Dissipative phase transition in a central spin system. *Phys. Rev. A* **86**, 012116 (2012).
64. Cai, Z. & Barthel, T. Algebraic versus exponential decoherence in dissipative many-particle systems. *Phys. Rev. Lett.* **111**, 150403 (2013).
65. Minganti, F., Biella, A., Bartolo, N. & Ciuti, C. Spectral theory of Liouvillians for dissipative phase transitions. *Phys. Rev. A* **98**, 042118 (2018).
66. Fitzpatrick, M., Sundaresan, N. M., Li, A. C. Y., Koch, J. & Houck, A. A. Observation of a dissipative phase transition in a one-dimensional circuit QED lattice. *Phys. Rev. X* **7**, 011016 (2017).
67. Rodriguez, S. R. K. et al. Probing a dissipative phase transition via dynamical optical hysteresis. *Phys. Rev. Lett.* **118**, 247402 (2017).
68. Fink, T., Schade, A., Hofling, S., Schneider, C. & Imamoglu, A. Signatures of a dissipative phase transition in photon correlation measurements. *Nat. Phys.* **14**, 365 (2018).
69. Zyczkowski, K., Horodecki, P., Sanpera, A. & Lewenstein, M. Volume of the set of separable states. *Phys. Rev. A* **58**, 883 (1998).
70. Vidal, G. & Werner, R. F. Computable measure of entanglement. *Phys. Rev. A* **65**, 032314 (2002).
71. Centrone, F., Mancino, L. & Paternostro, M. Charging batteries with quantum squeezing. <https://arxiv.org/abs/2106.07899>.
72. Konar, T. K., Patra, A., Gupta, R., Ghosh, S. & De, A. S., Multimode advantage in continuous variable quantum battery. <https://arxiv.org/abs/2210.16528>.
73. Rota, R., Minganti, F., Ciuti, C. & Savona, V. Quantum critical regime in a quadratically driven nonlinear photonic lattice. *Phys. Rev. Lett.* **122**, 110405 (2019).
74. Marty, G., Combrie, S., Raineri, F. & De Rossi, and A. Photonic crystal optical parametric oscillator. *Phys. Rev. Lett.* **15**, 53 (2021).
75. Macklin, C. et al. A near-quantum-limited Josephson traveling-wave parametric amplifier. *Science* **350**, 307 (2015).
76. Nigg, S. E., Lorich, N. & Tiwari, R. P. Robust quantum optimizer with full connectivity. *Sci. Adv.* **3**, e1602273 (2017).
77. Campaioli, F. et al. Enhancing the charging power of quantum batteries. *Phys. Rev. Lett.* **118**, 150601 (2017).
78. Gyhm, J.-Y., Šafránek, D. & Rosa, D. Quantum charging advantage cannot be extensive without global operations. *Phys. Rev. Lett.* **128**, 140501 (2022).
79. Downing, C. A. & Martín-Moreno, L. Polaritonic Tamm states induced by cavity photons. *Nanophotonics* **10**, 513 (2021).
80. Jaseem, N., Vinjanampathy, S. & Mukherjee, V. Quadratic enhancement in the reliability of collective quantum engines. *Phys. Rev. A* **107**, L040202 (2023).

Acknowledgements

Funding: C.A.D. is supported by the Royal Society via a University Research Fellowship (URF/R1/201158) and by Royal Society Enhanced Research Expenses, which support M.S.U. **Discussions:** We thank V.A. Saroka for fruitful discussions.

Author contributions

C.A.D. conceived of the study and wrote the first version of the paper, with revisions from M.S.U. Both C.A.D. and M.S.U. performed the calculations and gave final approval for publication.

Competing interests

The authors declare no competing interests.

Additional information

Supplementary information The online version contains supplementary material available at <https://doi.org/10.1038/s42005-023-01439-y>.

Correspondence and requests for materials should be addressed to Charles Andrew Downing.

Peer review information *Communications Physics* thanks Dario Rosa, Federico Centrone, and the other anonymous reviewer(s) for their contribution to the peer review of this work.

Reprints and permission information is available at <http://www.nature.com/reprints>

Publisher's note Springer Nature remains neutral with regard to jurisdictional claims in published maps and institutional affiliations.



Open Access This article is licensed under a Creative Commons Attribution 4.0 International License, which permits use, sharing, adaptation, distribution and reproduction in any medium or format, as long as you give appropriate credit to the original author(s) and the source, provide a link to the Creative Commons license, and indicate if changes were made. The images or other third party material in this article are included in the article's Creative Commons license, unless indicated otherwise in a credit line to the material. If material is not included in the article's Creative Commons license and your intended use is not permitted by statutory regulation or exceeds the permitted use, you will need to obtain permission directly from the copyright holder. To view a copy of this license, visit <http://creativecommons.org/licenses/by/4.0/>.

© The Author(s) 2023